CONFERENCE PRE-PRINT

THE HEAT LOAD DISTRIBUTION ON THE MAIN LIMITER DURING ICRF HEATING ON EAST

Binfu Gao¹, Rui Ding¹, Dahuan Zhu¹, Chuannan Xuan¹, Yang Wang^{1,2}, Bin Zhang¹, Pengfei Zi¹, Rong Yan¹, Chunyu He^{1,2}, Wenxue Fu^{1,2}, Cong Cao^{1,2}, Yifeng Zheng¹, Baoguo Wang¹, Junling Chen¹, and EAST team

¹ Institute of Plasma Physics, Chinese Academy of Sciences, Hefei, Anhui 230031, China

² University of Science and Technology of China, Hefei, 230031, China Email: binfu.gao@ipp.ac.cn;

Abstract

During ICRF heating, a large number of fast ions are generated, which can transport to far SOL and increase the heat load on the components located on the low field side. In recent campaigns on EAST, a lot of severe damage due to fast ions has been observed, including melting and macroscopic cracks. The radial width of the projection of the damaged area in the RZ plane is approximately 0.53 mm. It indicates that, when fast ions move to the radial position of the main limiter, their radial diffusion distance is very short, which is an important reason for the high heat load. The fast ion loss region is crescent-shaped in the poloidal direction and located on the ion side of the main limiter. As the core plasma density decreases and the ICRF power increases, the average energy of fast ion deposited on the main limiter increases, resulting a decrease in the poloidal width of the high heat load area. The ions with higher energy have a larger radial diffusion distance and can move deeply into the magnetic shadow of the main limiter. Finally, the heat load on the main limiter has been inversely calculated based on the time evolution of temperature. The results indicate that approximately 8.5% of the ICRF power is deposited on the main limiter, while the heat flux can reach up to 13.5 MW/m2. Increasing the core plasma density and the number of limiters can effectively mitigate the high heat load during high-power ICRF discharges.

1. INTRODUCTION

During the injection of the ion cyclotron resonance frequency (ICRF) power, ions can obtain large cyclotron speed [1], and be converted into trapped ions. Due to the stochastic ripple diffusion, they can move toward the low-field side [2], resulting in high local heat load on limiters [3]. The high heat load is an important factor restricting the increase of ICRF power in devices such as EAST [4], Alcator C-Mod [5], WEST [6], and JET [7].

On EAST, the main limiter is the closest plasma facing components (PFCs) to the last closed flux surface (LCFS) on the low field side under divertor equilibrium configurations. In 2022, three types of limiters with better thermal conductivity were tested: a tungsten-copper flat-plate limiter, a molybdenum limiter and a limiter with ITER-like tungsten-copper monoblock. During the discharges with high ICRF power, the 2-mm-thick tungsten tiles on the tungsten-copper flat-plate limiter bent and melted [8]. Macroscopic cracks and copper solidification layer were produced on the molybdenum tiles. The monoblock temperature exceeded the safety threshold.

Although limiters would be removed in future fusion device, the installation error of each module can reach up to 5 mm [9]. In some ways, the protruding modules also can be regarded as limiters. If the parallel heat flux decay width in the far SOL is around several or tens of centimeters, a 5 mm protrusion could be ignored. However, a recent study about 3D fast ion loss revealed that the radial width of the region where a large number of fast ions are lost can be less than 0.5 mm [10]. It means that even small protrusions can intercept a substantial number of fast ions, leading to severe local heat load. In future fusion devices, ICRF power is expected to reach tens of megawatts, which is about ten times the current ICRF power level on EAST. The high heat load may be a big challenge, which cannot be well predicted by simulation or semi-empirical functions [6].

In the paper, the characteristics of fast ion heat load on the surface of the main limiter are analyzed by using the infrared (IR) camera, which can provide data for the engineering design of the limiter and the study of fast ion transportation. The following is organized as: the geometry of the main limiter and the damage are introduced in Sections 2 and 3, respectively. Section 4 shows the poloidal and toroidal distributions of the fast ion heat load, and the total fast ions heat power deposited on the main limiter. Some methods used to mitigate the fast ion heat load are discussed in Section 5. Finally, a summary is made in section 6.

2. THE MAIN LIMITER

EAST is divided into 16 ports in the toroidal direction, while the major radius is 1.85 m and the minor radius is 0.45 m. The main limiter is positioned between the G and H ports in the low field side. The radial position is approximately 2350 mm in the midplane. The material is molybdenum from June to August in 2022. The mechanical design diagrams are shown in Fig. 1 (a) and (b). The height is 680 mm, and the width (toroidal direction) is 180.5 mm. There are 22 molybdenum tiles, the front face of each of which is tangent to a poloidal

arc of R = 750 mm. A schematic cross section of the molybdenum main limiter is shown in Fig. 1(c). The yellow areas represent the copper heat sink which has four cooling water tubes in the poloidal direction. The wine-red areas represent the molybdenum tiles. A through hole with a height of 7 mm and a width of 28 mm is designed in each molybdenum tile, which is used to place a copper block. A bolt through the heat sink is connected with the copper block.

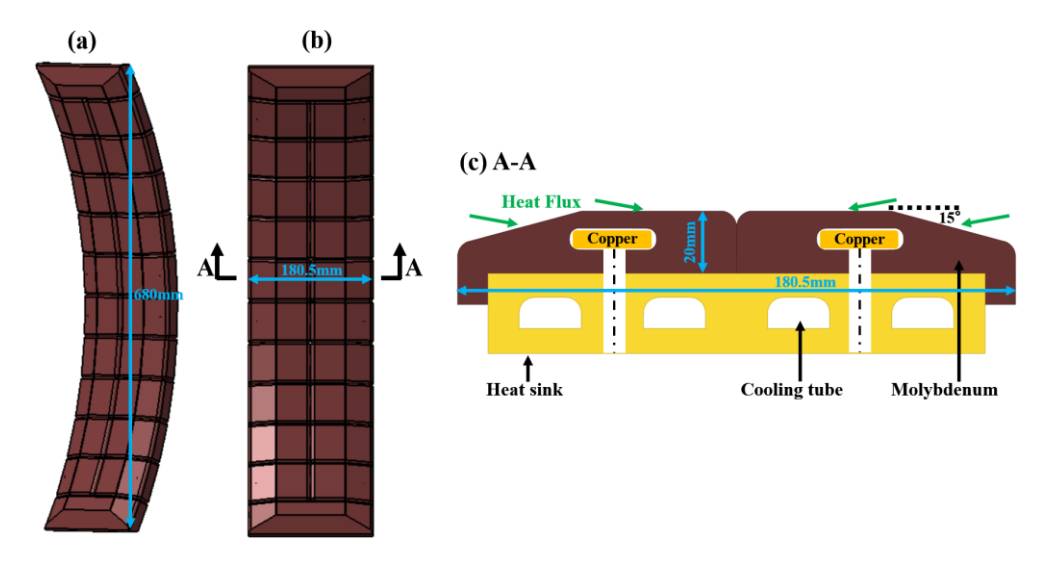


Fig. 1 The mechanical design diagrams of the molybdenum main limiter. (a) 3D view, (b) front view, (c) cutaway view of A-A

The main limiter can be monitored by two IR camera systems situated in the C and F ports [4], which are labelled as CIR and FIR, respectively. Both systems utilize 3-5 μ m middle wave IR cameras which are capable of measuring temperatures within the range of 0 to 2500 °C. These systems employ endoscopes equipped with reflective optics, allowing for a wide-angle view measuring 49.5° × 62° [11]. The distances between the end of endoscopes and the main limiters are approximately 3.88 m and 1.84 m, respectively. The spatial resolution is estimated to be about 6 mm for CIR camera and 1.3 mm for FIR camera.

3. THE DAMAGE ON THE MAIN LIMITER

Following the summer campaign in 2022, significant damage was observed on the main limiter, as illustrated in Fig. 2, including melting and cracking. Melting occurred on the copper block, indicating that the temperature of the entire molybdenum tile had exceeded the melting point of copper (1083.4 °C). The high temperature was found during 12-second discharges, implying that a substantial heat load was deposited on the tiles. The macroscopic cracks suggests that the damage is related to steady-state discharges. It is because that transient high-heat-flux events, such as plasma disruptions, typically cause only shallow surface cracks [12]. It should be noted that the cracks only can be found on the front surface of the tile. The radial width of the front surface is approximately 0.5 mm. It means a very short radial decay length of the high heat flux within the magnetic shadow region of the main limiter.

To clarify the reasons for the heat load, statistical analysis has been performed, in which the temperature at 2 s after the injection of ICRF was conducted. Fig. 3 (a) shows the most important factor is the ICRF power. In Fig. 3 (b), the temperature decreases with increasing core plasma density, while the ICRF power in each discharge is 1.1 MW. Besides, the temperature also decreases with the increase of the ratio of hydrogen to deuterium [4]. Similar phenomena have been observed in devices such as Alcator C-mod [5], Tore Supra [2]. The high temperature is thought to be caused by fast ions generated by ICRF waves. Although the fast ions are generated in the core plasma, they can transport to the far SOL and deposited on the main limiter. It is because ions can obtain high cyclotron velocity after interacting with ICRF waves. Then the passing particles can be converted into trapped particles [7]. Under stochastic ripple diffusion, the trapped ions move to the low field side [3]. When the trapped ions transport into the SOL, they cannot deposit on the upper or lower divertor targets via open magnetic field lines [13]. Instead, they continue moving along their trapped orbits until they are eventually trapped by the ripple field or loss on the components located on the low-field side [14]. As the ICRF power increases, the average energy of fast ions increases, which leads to an increase in the heat flux. On the contrary, as the core plasma

density increases, the probability of collisions between fast ions and electrons increases, resulting in a higher rate of fast ion loss through collisions. The fast ion flux deposited on the main limiter is reduced.

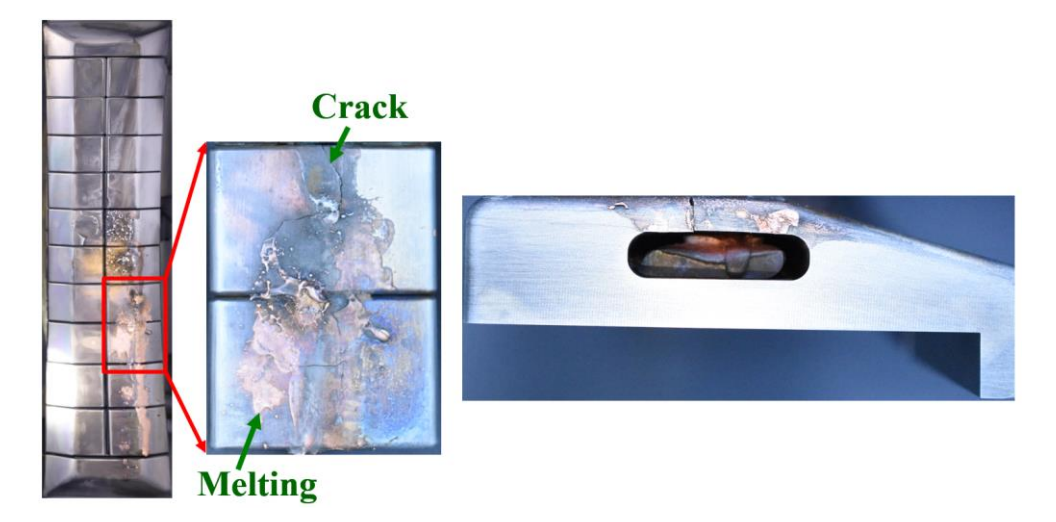


Fig. 2 The damage on the molybdenum limiter.

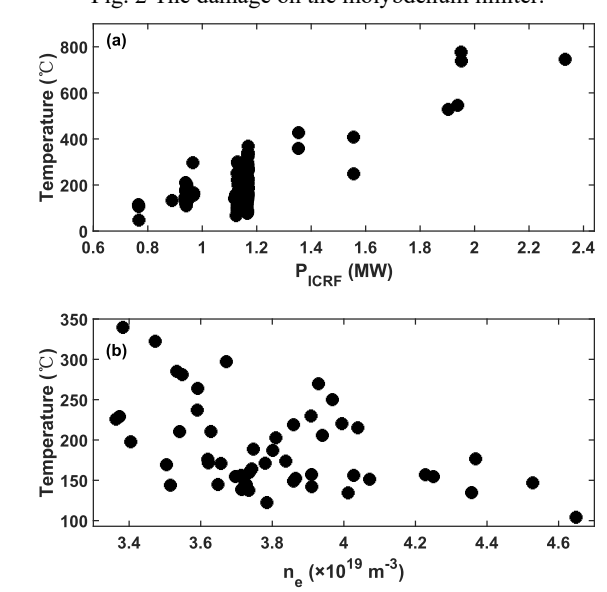


Fig. 3 The relationship between the main limiter temperature and ICRF power (a) and core plasma density (b), when the ICRF is injected for 2 s.

In recent years, EAST has made significant efforts to mitigate the temperatures on the main limiter. The main limiter has been upgraded to ITER-like tungsten-copper monoblock, which can withstand the heat flux of 10 MW/m². However, high temperatures remain an important factor restricting the achievement of high-power operation. One reason is that the spatial distribution characteristics of fast ion heat load is unclear.

4. THE CHARACTERISTICS OF FAST ION HEAT LOAD DISTRIBUTION

Three discharges with high ICRF power have been performed. The plasma current is 0.4 MA. The central line averaged plasma density is about 3.7×10^{19} m⁻³, while it is increased to 4.2×10^{19} m⁻³ during discharge of #112157. The powers of the 4.6 GHz low hybrid wave (LHW) and electron cyclotron resonance heating (ECRH) are 1.5 MW and 1.9 MW, respectively. The ICRF powers during discharges of #112150, #112151 and #112157 are 1.2 MW, 2.0 MW and 2.0 MW, respectively. The distance between the LCFS and the main limiter in the midplane is around 6.2 cm. The typical pictures observed by CIR and FIR are presented in Fig. 4. The main limiter and 4.6 GHz LHW guard limiters are located within orange and white dashed boxes, respectively. The blue dashed lines represent the location of mid-plane (MP). Two crescent-shaped, bright white regions can be observed simultaneously on both the main limiter and the 4.6 GHz LHW guard limiter, which means the temperature is very high.

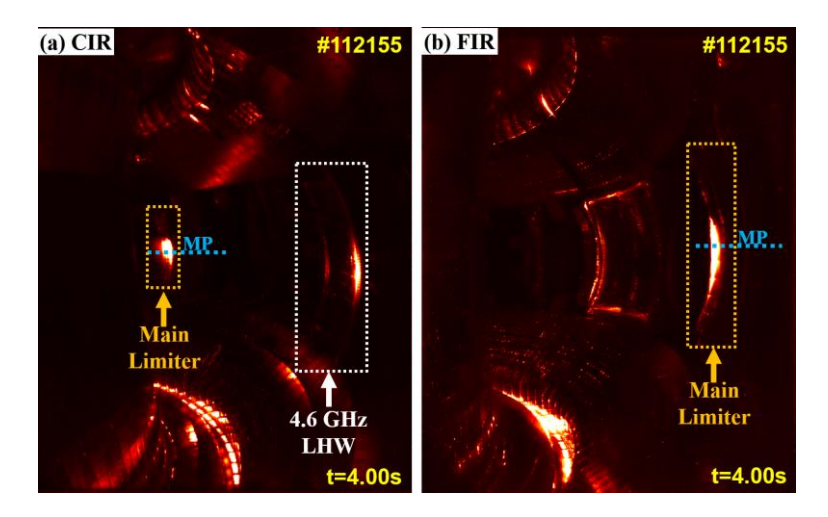


Fig. 4 The images captured by IR cameras at 4.00 s during discharge #112155. The images of (a) and (b) are captured by the IR cameras located at C port and F port, respectively. The main limiter is located within the orange dashed box, while the blue dashed line means the mid-plane.

4.1. The poloidal temperature distribution

The poloidal temperature distribution on the ion side of the main limiter is shown in Fig. 5, marked by black curve. The red curves calculated by PFCFlux code represent the heat power due to thermal plasma in the far SOL, while the decay length is assumed as 5 mm. If the heat flux in the far SOL is dominated by the background plasma, the maximum temperature of main limiter should be less than 200 °C. Comparing with the black line, it can be found that the fast ions are mainly deposited in the range of -230 mm to 100 mm.

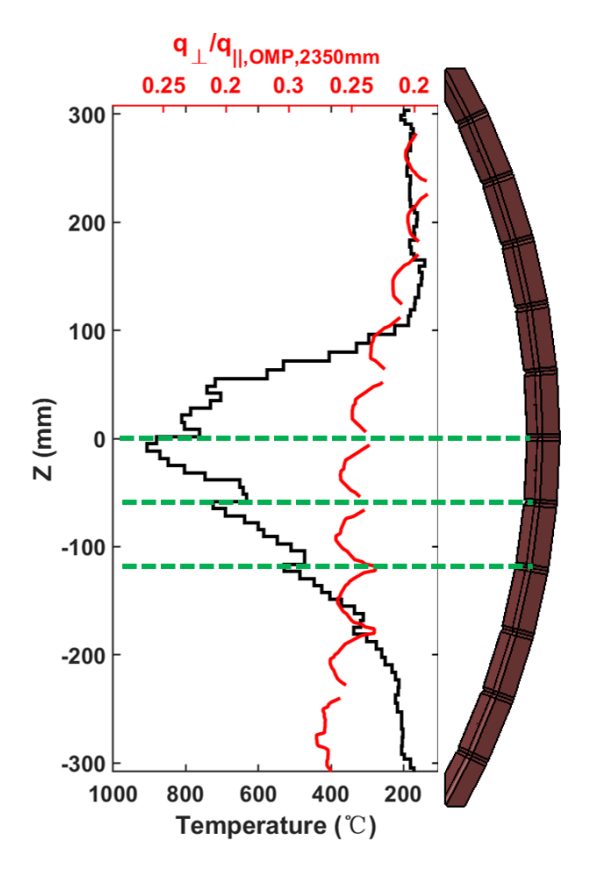


Fig. 5 The poloidal temperature distribution on the ion side of the main limiter.

The trajectories of fast ions have been traced by the Boris algorithm. Fig. 6 (a) displays the trajectories viewed from a top of the device, where the red and black curves represent the trajectories during two adjacent periods, respectively. Two observations can be made from the figure. Firstly, within a period, a fast ion circulates

toroidally for nearly three cycles. Secondly, after one period, a fast ion moves toroidally by approximately 215°. Besides, a radial walk of a hundred keV ion on EAST is about tens of microns [15]. All of them are the main reason for the short radial width of the heat flux in the magnetic shadow of main limiter.

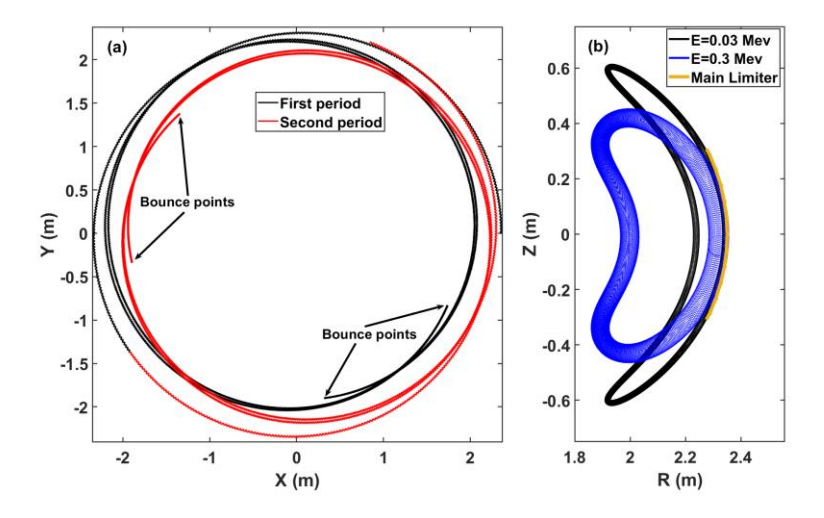


Fig. 6 The trajectories of hydrogen ions. (a) viewed from the top of device and (b) projection of the trajectory in the RZ plane.

Fig. 6 (b) shows the projection of the trajectories of fast ions with energies of 30 keV and 300 keV in the RZ plane, where the orange curve represents the main limiter. It can be found that as the energy of the fast ions increases, the trajectories contract toward the mid-plane. It means that the poloidal width of the fast ion loss region varies with their energy. The peaking temperature profile in Fig. 5 seems to indicate that fast ions with different energies are deposited on the surface of the main limiter.

When the plasma density increases from 3.7×10^{19} m⁻³ to 4.2×10^{19} m⁻³, there are three noticeable changes in the poloidal temperature distribution, as shown in Fig. 7 (a). First, the maximum temperature decreases from 1264 °C to 754 °C. Second, the position of peak is shifted from -50 mm to 0 mm. Finally, the full width at half maximum of the temperature profile decreases from 260 mm to 216 mm. However, the poloidal temperature distribution of the 4.6 GHz LHW guard limiter remains almost unchanged, as presented in Fig. 7 (b).

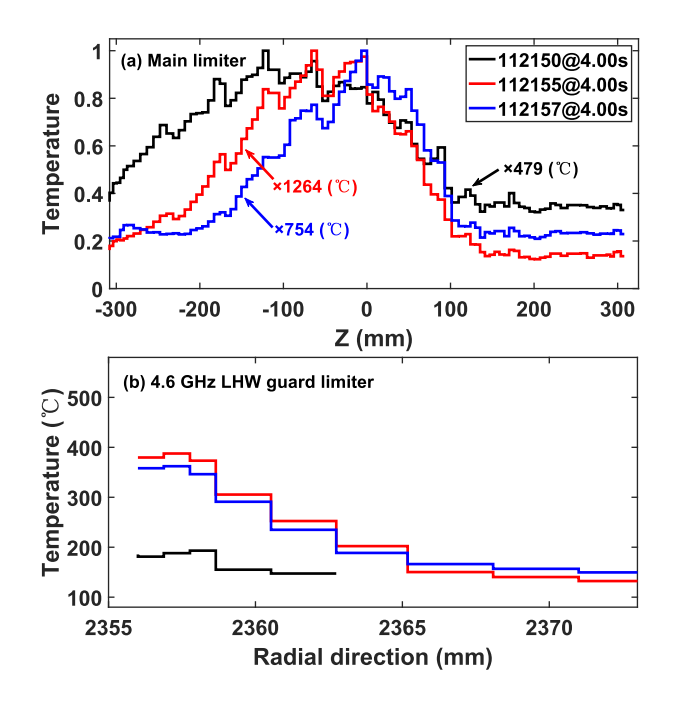


Fig. 7 The temperatures of main limiter (a) and 4.6 GHz LHW guard limiter (b) during discharges of #112155 and #112157 at 4.00 s.

As the plasma density increases, the rate of fast ions being lost through collisions rises, resulting in low heat fluxes deposited on the limiters [16]. However, the nearly constant temperature on the $4.6 \, \text{GHz}$ LHW guard limiter suggests that there is less effect of collisions on the fast ion generation and transportation. It is because that the collision rate is proportional to $1/v^3$, the ions with lower energy are more likely to be lost through collisions. The $4.6 \, \text{GHz}$ LHW guard limiter (located at E-port) and the main limiter are toroidally spaced by 45° , and the radial position of the $4.6 \, \text{GHz}$ LHW guard limiter is approximately 6 mm larger than that of the main limiter. Thus, the $4.6 \, \text{GHz}$ LHW guard limiter is within the magnetic shadow of the main limiter. Since the radial walk is proportional to the ion gyro-radius [15], only ions with sufficiently high energy can traverse the 6 mm radial distance and deposit onto the $4.6 \, \text{GHz}$ LHW guard limiter. The change in the poloidal temperature distribution on the surface of the main limiter is primarily due to a reduction in the total fast ion flux, accompanied by an increase in the average energy.

When the ICRF power is increased from 1.2 MW to 2.0 MW, the temperature of both the main limiter and the 4.6 GHz LHW guard limiter is increased significantly. The peak location of the poloidal temperature distribution on the main limiter shifts to the mid-plane. The full width at half maximum of the temperature profile decreased from 387 mm to 260 mm. With the increase of ICRF power, the average energy of H ions increases when the concentration of H ions is constant. The heat flux deposited onto the limiters is significantly increased.

4.2. The poloidal temperature distribution

A typical toroidal distribution of temperature at Z=-30 mm is presented in Fig. 8 (b), marked by black curve. The red dots represent the heat load from thermal plasma in the far SOL, which is calculated using the PFCFlux code with a decay width of 5 mm. The thermal plasma heat load is mainly deposited on the bevel and symmetric. On the contrary, the fast ions mainly loss on the front face of the tiles, where the damage occurs. It confirms the small radial width of the fast ion heat flux. Additionally, the fast ions are mainly lost on the right side of the main limiter. It is because, the on the low-field side, the direction of the toroidal velocity of trapped ions is the same as that of the plasma current, leading to predominant deposition on the ion side.

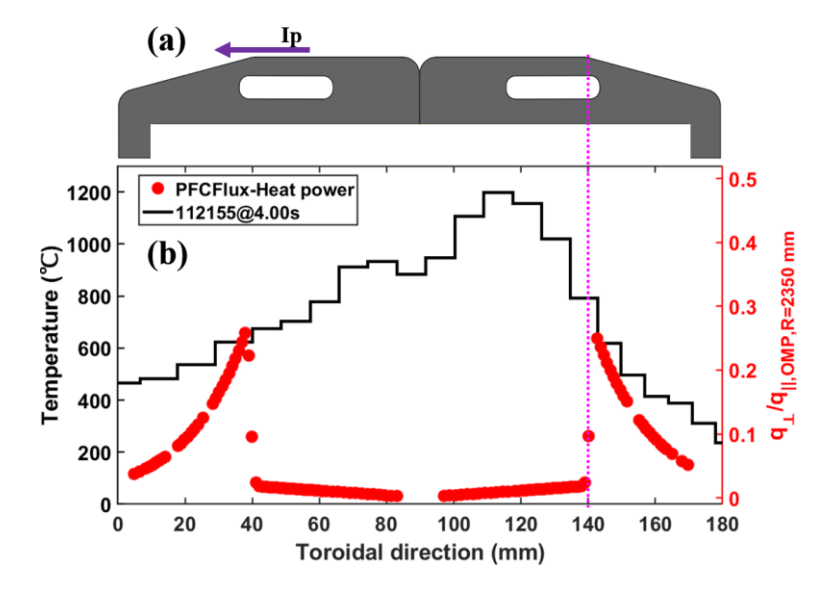


Fig. 8 The schematic cross section of the main limiter at Z=-30 mm (a) and the toroidal distribution of temperature (black line) and heat power (red dots) at Z=-147 mm (b).

4.3. The poloidal temperature distribution

In this section, the heat power profile is evaluated by ANSYS program based on the temperature profile measured by the IR camera. In ANSYS program, a 3D molybdenum tile model has been established, whose shape and size are the same as those of the real. The specific heat capacity and thermal conductivity are the same those of molybdenum material, which are a function of temperature. They are 205 J/(kg • K) and 142 W/(m • K) at 20 °C. The density is 10200 kg/m³. On the front face, the heat flux distribution function is obtained by fitting the temperature profile. On the bevel and side, the heat flux decays exponentially along the radial direction. In thermal simulation, the heat flux is

assumed to be imposed within 2 s after ICRF injection and the initial temperature of the model is 20 °C. The radiation on the front face, bevel and side has been considered.

Fig. 9 shows the heat flux profiles after the injection of ICRF waves. It is surprising that the peak heat flux reaches up to 13.5 MW/m². Secondly, the heat flux deposited on the front face of the molybdenum tiles is significantly greater than that deposited on the bevel, even though the incident angle on the bevel is much larger than that on the front face. Finally, the peak heat flux is located near 110 mm in the toroidal direction, indicating that the radial diffusion distance of many fast ions within the magnetic shadow region of the main limiter is approximately 0.26 mm.

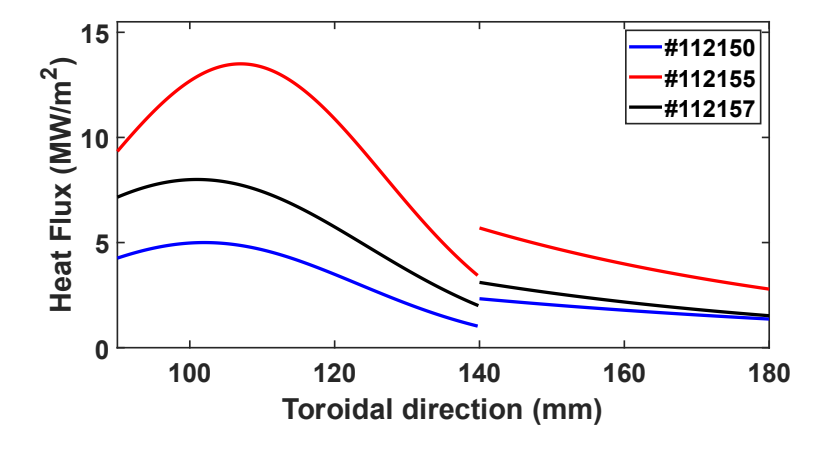


Fig. 9 The heat power distribution inverse calculated from the temperature.

From Fig. 4, it can be found that the fast ions are primarily deposited on the 4th to 9th molybdenum tiles located at the right of the main limiter, while the midplane is located between the 5th and 6th tiles. Thus, based on the temperatures on the surfaces of these tiles, six heat flux profiles at different poloidal position have been obtained. Tab. 1 shows the total heat power on each tile. The total heat power of fast ions on the main limiter was about 0.17 MW, accounting for 8.5% of the total ICRF power.

Tub. 1 The total heat power on each the totaled at foil state during also harge of #112155.							
No	4	5	6	7	8	9	Total
Heat power (MW/m²)	0.014	0.026	0.040	0.044	0.029	0.017	0.17

Tab. 1 The total heat power on each tile located at ion side during discharge of #112155.

To address the high heat load issue, many mitigation methods have been explored. In experimental, the high heat load can be mitigated by increasing the core plasma density and the ratio of hydrogen to deuterium [4]. But the benefits are limited. It is because the density should not be much greater than Greenwald density. And the fraction of collision loss decreases with increasing particle energy, while the average energy increases with the ICRF power. For good coupling, the hydrogen minority concentration should be between 5% and 15% [17].

In engineering, the main limiter was upgraded to ITER-like tungsten-copper monoblock in 2022 [18], which can withstand heat fluxes of up to 10 MW/m². Besides, the profile was also optimized to decrease the peak heat flux. The angle between the surface and the magnetic field lines was reduced to 5°. Nevertheless, the improvement is limited. A significant reason is that the installation error of tungsten monoblock strings is 0.5 mm, which is comparable to the radial width of the high thermal load region. As a result, the heat flux is primarily deposited on the most protruding tungsten monoblock string.

During ICRF heating, a lot of fast ions can be absorbed by the 4.6 GHz LHW guard limiter. And the average energy of fast ions deposited on the 4.6 GHz LHW guard limiter is higher than that of fast ions deposited on the main limiter. As the ICRF power increases, the average energy of fast ions will further rise. Hence, additional limiters are required to distribute the fast ion heat flux.

5. SUMMARY

In recent years, severe damage has been observed on the main limiter due to fast ions generated by ICRF. The damage mainly occurs on the front face of the molybdenum tiles, whose radial width is around 0.53 mm. It suggests a narrow width in the radial heat flux distribution in the magnetic shadow. The short width is mainly related to the slower diffusion speed, faster toroidal precession speed, and broader range of toroidal motion in one period. The high heat load regions caused by fast ions appear on the ion side. There is strong effect of the core plasma density and ICRF power on the poloidal length of the high heat load region, because of the change in the average energy of the fast ions deposited on the main limiter. The inverse calculation shows the heat load reaches up to 13.5 MW/m² and approximately 8.5% of the ICRF power is deposited onto the main limiter through fast ion losses. The narrow width and extremely high peak values make the heat load impossible to be mitigated through engineering design, while it can be reduced by increasing the core plasma density. Increasing the number of limiters can significantly reduce the heat load from higher-energy fast ions.

ACKNOWLEDGEMENTS

The work was supported by National Key R&D Program of China under Contract Nos. 2022YFE03030000, 2022YFE0109700 and 2024YFE03000200, the Anhui Provincial Natural Science Foundation (contract no. 2208085J40), the programs of National Natural Science Foundation of China (Nos. U21A20439, 12505240, 12425509, U24A2020, 12205332, 12405243 and 12205333), the Strategic Priority Research Program of Chinese Academy of Sciences under Grant No. XDB0790103, the CASHIPS Director's Fund with Grant No. JPY2023A03, the HFIPS Director's Fund with Grant Nos. YZJJ2024QN24 and Anhui Provincial Major Science and Technology Project 2023z020004.

REFERENCES

- [1] M. J. Mantsinen, L. G. Eriksson, et al., Evidence for regions of nearly suppressed velocity space diffusion caused by finite Larmor radius effects during ICRF heating, Nuclear Fusion, 39 (1999) 459-466.
- [2] V. Basiuk, L. G. Eriksson, et al., Ripple losses during ICRF heating in Tore Supra, Nuclear Fusion, 44 (2004) 181-192.
- [3] Y. Ikeda, K. Tobita, et al., Ripple enhanced banana drift loss at the outboard wall during ICRF/NBI heating in JT-60U, Nuclear Fusion, 36 (1996) 759-767.
- [4] B. F. Gao, D. H. Zhu, et al., Modeling of heat flux on the main limiter in EAST, Nuclear Fusion, 65 (2025) 086005.
- [5] A. N. James, D. Brunner, et al., Imaging of molybdenum erosion and thermography at visible wavelengths in Alcator C-Mod ICRH and LHCD discharges, Plasma Physics and Controlled Fusion, 55 (2013) 125010.
- [6] D. Moiraf, J. Morales, et al., Optimization of the operational domain for ICRH scenarios in WEST from statistical analysis, Nuclear Fusion, 63 (2023) 086010.
- [7] V. G. Kiptily, C. P. P. von Thun, et al., Recent progress in fast ion studies on JET, Nuclear Fusion, 49 (2009) 065030.
- [8] C. N. Xuan, D. H. Zhu, et al., Melting of W/Cu flat type component for main limiter and its impact on plasma operation in EAST experiments, Nuclear Fusion, 64 (2024) 086039.
- [9] G. Xu, H. Wang, et al., Estimation of heat load distribution and W erosion on the CFEDR first wall, Plasma Science and Technology, 27 (2025) 104010.
- [10] Y. Zheng, W. Zhang, et al., 3D simulation of orbit loss and heat load on limiters of ICRF-NBI synergy induced fast ions on EAST, Nuclear Fusion, 63 (2023) 046016.
- [11] R. R. Liang, X. Z. Gong, et al., Investigation of divertor heat flux characteristics under the influence of resonant magnetic perturbations on EAST, Nuclear Fusion, 65 (2025) 026021.
- [12] C. N. Xuan, D. H. Zhu, et al., First analysis of in-situ melting on TZM tiles at high field side of the first wall in EAST, Nuclear Materials and Energy, 34 (2023) 101377.
- [13] G. J. Kramer, R. V. Budny, et al., A description of the full-particle-orbit-following SPIRAL code for simulating fast-ion experiments in tokamaks, Plasma Physics and Controlled Fusion, 55 (2013) 025013.
- [14] A. Ekedahla, J. Bucalossi, et al., Operational limits during high power long pulses with radiofrequency heating in Tore Supra, Nuclear Fusion, 49 (2009) 095010.
- [15] G. Park and C. S. Chang, Numerical study of collisional ripple diffusion in a tokamak plasma, Physics of Plasmas, 10 (2003) 4004-4015.
- [16] J. M. Faustin, W. A. Cooper, et al., Fast particle loss channels in Wendelstein 7-X, Nuclear Fusion, 56 (2016) 092006.
- [17] X. J. Zhang, H. Yang, et al., First experimental results with new ICRF antenna in EAST, Nuclear Fusion, 62 (2022) 086038.
- [18] Z. X. Guo, D. H. Zhu, et al., Long-term plasma exposure of ITER-like W/Cu monoblocks with pre-damaged surfaces in EAST experiments, Nuclear Fusion, 64 (2024) 076026.